NASA
Technical
Paper
2650

March 1987

# Correlation of Helicopter Impulsive Noise From Blade-Vortex Interaction With Rotor Mean Inflow

Andrew B. Connor
and R. M. Martin

**NASA Technical Paper 2650**

1987

# Correlation of Helicopter Impulsive Noise From Blade-Vortex Interaction With Rotor Mean Inflow

Andrew B. Connor
and R. M. Martin

*Langley Research Center*
*Hampton, Virginia*

National Aeronautics
and Space Administration

**Scientific and Technical Information Branch**

## Summary

Data from a test made in the Langley 4- by 7-Meter Tunnel were parametrically studied with respect to the occurrence of blade-vortex interaction (BVI) as a function of tunnel speed and rotor angle of attack. Three microphones on the tunnel centerline forward of the model and one microphone forward and 45° to the right provided the data for this study. The rotor model was tested with a set of high-twist blades (−10°) and a set of low-twist blades (−5°) over the midspeed range (50 to 80 knots) at angles of attack ranging from −6° (shallow climb) to 10° (steep descent). The data from all four microphones indicated that the most probable time of occurrence of BVI is when the rotor descent is approximately equal to the rotor mean inflow velocity. However, some of the data showed no conclusive relationship to the mean inflow velocity.

## Introduction

Helicopter impulsive noise from blade-vortex interaction (BVI) is a well-known lifting rotor phenomenon that develops when a lifting rotor blade impinges local vortices within the rotor flow field. This impingement generates a characteristic pressure pulse—one that sharply rises and sharply decays, thus writing an impulse signature that is readily identified from acoustic pressure time histories. Furthermore, there are some rotor operating regimes wherein the BVI impulsive noise is quite intense in contrast to other operating regimes where the BVI impulse is not perceptible.

The BVI phenomenon has been studied by a number of investigators both in flight tests and in wind tunnels, the general purpose of which has been to determine the physical mechanism that generates the impulsive sound as well as to study its general physical characteristics such as radiation patterns, intensity levels, etc. One characteristic result of these studies has been contours of impulsive noise levels plotted as a function of flight speed and rate of descent. Wind-tunnel data were obtained from the tunnel analogy of those parameters: tunnel speed and rotor drag. The resulting contours were somewhat irregular in shape and have been likened to a "fried egg" pattern by some analysts. A collateral aspect of these studies was to develop an operational avoidance flight envelope if such were to prove feasible from the data. Typical examples of these works are described in references 1 through 4.

To gain some insight into the operating regime/BVI occurrence, model test data from the Langley 4- by 7-Meter Tunnel were analyzed from two nominally 9-ft-diameter lifting rotors. (See refs. 5 and 6.) This test was part of a series of helicopter rotor noise tests, and the results of this study make up one element of that research.

The two four-blade rotor models differed slightly in disk loading and blade planform. Each rotor was studied with variable tip configurations, but the significant difference between the rotors for this study was a difference in twist distribution. One rotor was twisted −10° and the other −5°. In this paper the framework of the rotor operating regime is the forward-speed/angle-of-attack combination, whereas the normal framework in full-scale powered flight is the forward-speed/rate-of-descent combination. Rate of descent, however, is not a measured wind-tunnel parameter but must be inferred from angle-of-attack data.

Also, there were indications of directionality from the data. These directional characteristics will be identified by the statistics of the impulsive sounds and by the loci of the microphones when the sounds were recorded.

## Symbols and Abbreviations

Conventional helicopter symbols and terminology will be employed throughout this paper in the discussions about and descriptions of these test rotors. (See ref. 7.) Values are usually given in U.S. Customary Units, but they are occasionally given in SI units or in both where considered useful. Measurements and calculations were made in U.S. Customary Units.

| | |
|---|---|
| BVI | blade-vortex interaction |
| DL | disk loading, Rotor thrust/Rotor swept area, $lb/ft^2$ |
| $dp(+)$ | pressure in positive direction, $dynes/cm^2$ |
| $dp(-)$ | pressure in negative direction, $dynes/cm^2$ |
| $dt$ | time increment, sec |

| | |
|---|---|
| $\ell$ | distance from center of rotor tip path plane to microphone, measured in rotor tip path plane, $\left(x^2+y^2\right)^{1/2}$, ft |
| $R$ | rotor radius, 4.67 ft |
| $r$ | radial distance from center of rotor tip path plane to microphone, $\left(x^2+y^2+z^2\right)^{1/2}$, ft |
| $r/R$ | fraction of rotor radius |
| $T$ | rotor thrust, lb |
| $V$ | forward flight velocity, wind-tunnel speed, knots |
| $\bar{v}_i$ | rotor mean inflow velocity, $(\mathrm{DL}/2\rho)(1/V)$ |
| $x$ | microphone coordinate relative to center of rotor tip path plane, positive upstream |
| $y$ | microphone coordinate relative to center of rotor tip path plane, positive to left looking upstream |
| $z$ | microphone coordinate relative to center of rotor tip path plane, positive up |
| $\alpha_{\mathrm{TPP}}$ | rotor tip-path-plane angle, positive when vehicle nose is up, deg |
| $\gamma$ | angle of climb, deg |
| $\theta$ | polar angle, angle down from rotor tip path plane, positive downward, $\tan^{-1}(z/\ell)$, deg |
| $\rho$ | air density |
| $\psi$ | azimuth angle, angle in plane of rotor, positive counterclockwise, zero over aircraft tail, $\tan^{-1}(y/x)$, deg |

## Description of Experiment

### Wind-Tunnel Facility

The dimensions of the rectangular eductor (nozzle) of the Langley 4- by 7-Meter Tunnel when operated as an open-throat test chamber are 4.42 m (14.50 ft) high and 6.63 m (21.75 ft) wide. The ceiling of the test chamber in the open-throat configuration is approximately 7.50 m (24.60 ft) above the test chamber floor. The floor of the test section remains in place so that three sides of the jet are open.

The ceiling was treated with 4-in. acoustic foam, and the floor was treated with 6-in. fiberglass insulation covered by perforated sheet. The sidewalls and floor out of the flow, in the vicinity of the microphones, were also covered with acoustic absorptive material to reduce the effects of reflected signals. The rotor model and test rig in the open-throat test chamber are shown in figure 1. The acoustic treatment is visible in this figure as well.

Standard NASA measuring systems for rotor, wind tunnel, and acoustics with signal processing and computer interfacing were employed for this test and are described in detail in reference 6.

### Rotor Model System

Two four-blade rotor models were tested upon the General Rotor Model System (GRMS) (ref. 4). Details of the two rotor models are presented in figure 2 which shows their planform and twist. Other pertinent data for these models are listed in table I. The fuselage model employed had a generic fuselage shape of approximately the correct scale for this size rotor.

### Microphone Positions

Figure 3 is a layout sketch showing the positions of the various microphones for this experiment. The microphones from which the data were acquired for this report will be identified by number throughout according to the list below and as shown in figure 3. This list shows the microphone position relative to the rotor hub at a fixed position within the wind-tunnel test section. Notice that these positions coincide with

standard rotor notation where $\psi = 0°$ is over the tail boom and $\psi = 90°$ is on the advancing blade tip. Here, $r$ denotes the radial distance from the hub to the microphone, $\theta$ is positive downward from the plane of the rotor, and $\psi$ denotes the azimuth angle.

| Microphone | $r$, ft | $\theta$, deg | $\psi$, deg |
|---|---|---|---|
| 3 | 8.28 | 44 | 176 |
| 4 | 13.99 | 13 | 172 |
| 5 | 14.52 | 23 | 177 |
| 12 | 12.98 | 25 | 133 |

Also, when the model angle of attack was changed, the physical location of the rotor hub in the test section varied slightly because it pivoted about a reference point approximately 29 in. below the rotor hub.

### Test Procedure

***Test conditions.*** The research objective was to map the BVI impulsive noise as a function of forward speed and rotor tip-path-plane angle at fixed thrust coefficient for each rotor configuration. Although a wider range of tunnel speed was of interest, tunnel characteristics described in reference 1 limited the speed for this test to a range between 50 and 80 knots. Rotor tip-path-plane angles ranged from $-6°$ to $10°$. The overall test plan was thus a matrix of the variation of velocity with tip-path-plane angle at discrete increments. The rotor test matrices as actually implemented are shown in figure 4. The range of rotor angle was intended to bracket the regions of BVI noise from its onset through the maximum at each flight speed.

***Rotor control and performance.*** The mean velocity of the tunnel free stream was corrected for open-jet boundary effects using the theory of reference 8. Rotor angles of attack were therefore adjusted during the run for the actual tunnel flow conditions. Collective pitch was adjusted after each angle-of-attack change to maintain a constant thrust coefficient, and cyclic pitch was adjusted to maintain zero flapping and thus assure that rotor shaft angle of attack was equal to rotor tip-path-plane angle of attack.

The performance data were acquired simultaneously with the acoustic data in order to relate the character of the noise to rotor operating parameters. Upon achieving a steady-state operating condition, all data were acquired and stored for later processing. All the rotor operating data for this report are referenced to corrected tunnel speed (see ref. 8) and corrected rotor angle of attack. Rotor angle of attack provides rate of climb by computation where there are no unaccounted for drag forces.

***Acoustic data reduction.*** The analog signals were digitized by a conditional sampling technique based on the rotor once-per-revolution signal. A synchronizer sampled the signals at 1024 equally spaced intervals during one revolution so that the 1024 points defining each rotor revolution are at the same relative phase. The synchronizer also adjusted for small changes in rotor speed. The acoustic time histories of 50 rotor revolutions were sampled in this manner and then ensemble-averaged to obtain an average acoustic waveform and standard deviation for each test condition. The effect of this averaging technique is to remove random fluctuations such as background noise and to enhance the periodic content of the signal.

## Analysis

### BVI Pulse Shape

BVI impulses are identified by the shape of the acoustic pressure time history. Figure 5(a) shows a typical BVI impulse. The characteristic curve is a steep-gradient positive pressure followed by an equally steep-gradient negative pressure; this is seen clearly in the figure. A typical nonimpulsive time history is shown by figure 5(b). Figure 5 is a pressure time history of one rotor revolution where pressure is in dynes/cm$^2$, and time is shown in fractions of a rotor revolution. This example from the low-twist rotor and the fuselage-mounted microphone is at $V = 70$ knots and $\alpha_{TPP} = \pm 2°$. This case from the fuselage microphone is presented to clarify the contrast between two adjacent test points. Similar examples of rotor-generated BVI impulses showing the same characteristic shape from both model and flight data are presented in references 3 and 4.

### Acoustic Data Search and Sort

The entire acoustic time history data base from microphones 3, 4, 5, and 12 was searched and sorted using software by the criteria listed below for time history characteristics similar to the example shown by figure 5(a).

Selection of the three levels for the search criteria was an engineering judgment derived from visually evaluating quantities of rotor acoustic pressure time histories. These three criteria essentially define three increasing levels of BVI impulsive content in the time signals. These criteria were applied to the pressure increase ($dp(+)$) and the pressure decrease ($dp(-)$) exhibited by the time histories within a specified time increment ($dt$) as follows:

| | Microphones 4, 5, and 12 | | Microphone 3 | | All microphones |
|---|---|---|---|---|---|
| Criterion | $dp(+)$, dynes/cm$^2$ | $dp(-)$, dynes/cm$^2$ | $dp(+)$, dynes/cm$^2$ | $dp(-)$, dynes/cm$^2$ | $dt$, sec |
| 1 | 120 | 80 | 210 | 140 | 0.00040 |
| 2 | 160 | 120 | 280 | 210 | .00053 |
| 3 | 200 | 160 | 351 | 280 | .00066 |

The computer routine first processed the data according to criterion 3, then according to criterion 2, and then 1. Different pressure criteria were applied for microphone 3 because microphone 3 was at two-thirds the distance of microphones 4, 5, and 12. The pressure increase and decrease criteria were therefore proportionately multiplied by $1/r$ under the acoustical far-field assumption. The far-field assumption is valid for the BVI phenomenon because of its frequency content and very localized source region.

The data were searched for conditions exhibiting a pressure increase of $dp(+)$ with a pressure gradient (slope) of $dp(+)/dt$ and subsequently a pressure decrease of $dp(-)$ with a pressure gradient of $dp(-)/dt$. The negative and positive pressure gradients are the same for all three criteria. In addition to the positive and negative amplitude and slope criteria, a time frame window was also considered. This additional criterion was essential to the analysis because not every time history with a steep pressure increase was followed immediately by a steep pressure decrease. Therefore, the search algorithm required that the positive and negative slopes, hence the pulse, occur sequentially within 0.05 of a rotor rotation.

### Rotor Operating Regime

The operating regime BVI dependence is evaluated in terms of impulsive acoustic signal levels and rotor tip-path-plane angle of attack versus forward speed. The rotor operating data were extracted from the wind-tunnel data base for correlation with the BVI impulse data as depicted by the sample from the low-twist rotor shown in table II. In addition to rotor operating parameters, table II shows the actual $dp(+)$ amplitude of the BVI pulse at the time and duration of occurrence expressed as a fraction of one rotor rotation. One should also note that although there are four blade passages for each rotation, the search algorithm was structured such that a BVI impulse occurring at any blade passage was sufficient to satisfy the selection criterion, and the search routine would step to the next case. Therefore, subsequent blade passages were not evaluated even though they might have generated a BVI impulse. It was beyond the scope of this work to evaluate variations in BVI level between successive blade passages.

## Results and Discussion

The following discussion relates primarily to the question of BVI impulse occurrence as a function of rotor operating regime and secondarily to the trend of apparent directivity as deduced from the fixed loci of the microphones.

### Data Trends

Although rotor operation in the wind tunnel was limited by practical constraints to a speed range from 50 to 80 knots, the data are sufficient to draw some inferences about BVI impulse occurrence with respect to the rotor operating regime. The trend of these data suggests that rotor blade-vortex impingement which causes impulsive interaction noise is more likely to occur when the rotor descent rate approaches the descent rate of the rotor flow field, which is the mean downwash velocity.

All the sorted BVI data from both rotor models were plotted as functions of $\alpha_{TPP}$ versus tunnel speed for each of the four microphones. These plots are shown in figures 6 and 7 for the low-twist and high-twist blades. Approximately half the BVI impulses were greater than 200 dynes/cm$^2$, and those cases are indicated

by the shaded symbols in each figure. The format of these figures is intended to conform generally with the format of flight test data where noise level boundaries are plotted in terms of velocity versus rate of climb as in reference 3. The data points were therefore bounded in approximate contours forming similar plots. Superposed on these figures is the curve of $\bar{v}_i$ which shows a negative rate of climb. The higher level impulses cluster about this curve, whereas the lower level impulses tend to scatter away from it. References 3 and 4, for example, have shown a similar dependence between the descent-rate/forward-speed combination of the lifting rotor and integrated sound pressure levels. Note that in conformity with helicopter sign convention, $\alpha_{TPP}$ becomes more positive as the rate of climb becomes more negative.

In order to satisfy the momentum equation, the total rotor flow including the blade tip vortices will be driven downward with the rotor wake. However, the wake sink rate is essentially equal to the rotor mean inflow when still very close to the rotor plane (within the time lapse between two successive blade passes, long before the slipstream is able to develop fully). Rotor mean inflow, in turn, is fairly easily approximated. A method for estimating both the rotor mean inflow velocity and negative rate of climb is provided below.

### Approximation of Mean Inflow and Rate of Climb

The rate of descent for any combination of tip-path-plane angle and forward velocity can be approximated from the ratio of rotor drag to rotor lift where Drag $= T \sin \alpha_{TPP}$, and Lift $= T \cos \alpha_{TPP}$, provided that there are no extraneous forces in the system. From reference 7 (eq. (16) in ch. 9), the angle of climb $\gamma$ is equal to the tangent of drag over lift; thus, the rate of climb is equal to $V\gamma$. Rotor mean inflow velocity is readily approximated from momentum considerations as a function of disk loading and as an inverse function of forward velocity. (See, for example, the appendix in ref. 9.) Thus, in the same manner, if the thrust is known, disk loading is readily computed and the rotor mean inflow is derived from it.

### Directivity

The low-twist rotor and the high-twist rotor exhibited different distributions of impulse level as a function of microphone position. These variations are also shown by figures 6 and 7 and the summary of statistical data provided in table III. For each rotor set these data indicate some directional trends: most impulses were recorded at microphones 12 and 5 ($\theta = 25°$ and 23°, respectively) and not as many impulses were recorded at microphones 3 and 4 ($\theta = 44°$ and 13°, respectively). Although microphones 4 and 5 were located essentially at the same azimuth angle (approximately 180°) and their radial distances were nearly equal, there were double the number of impulse occurrences at microphone 5 than at microphone 4 for both low- and high-twist blades. The data listed below are extracted from the same source as table II, and their acoustic pressure time histories are plotted in figure 8. This list is typical of the data acquired during this study.

| $V$, knots | $T$, lb | $\alpha_{TPP}$, deg | Microphone | BVI, dynes/cm$^2$ | Time of occurrence, fraction of rotation |
|---|---|---|---|---|---|
| 71.13 | 480.11 | 4.58 | 3 | 305.9 | 0.370 to 0.378 |
| 71.13 | 480.11 | 4.58 | 4 | 129.1 | .729 to .736 |
| 71.13 | 480.11 | 4.58 | 5 | 274.4 | .496 to .505 |
| 71.13 | 480.11 | 4.58 | 12 | 207.7 | .144 to .150 |

Analysis of the rotor rotation in every data set started and ended simultaneously for all microphones. In this case, however, the nearest microphone (3) was not the first to record the impulse; also, the farthest microphone (5) was not the last to record the impulse. Although the cause is not altogether clear, a reasonable supposition is that the rotor blades, following each other, do not identically encounter the numerous vortex packets within the flow field. This effect is to be expected because the shed vortices will vary from blade to blade and the flow field itself is somewhat variable.

## Concluding Remarks

A rotor noise and performance experiment was undertaken in the Langley 4- by 7-Meter Tunnel with two rotor models comprising nine configurations. Tests were conducted over the midvelocity range from 50 to 80 knots and through rotor angles of attack from −6° to 10°.

A higher level of impulsive noise from blade-vortex interaction (BVI) occurred at combinations of rotor tip-path-plane angles of attack and forward flight speeds with the result that the inferred rate of descent approximated the rotor mean inflow velocity.

Data from four microphones positioned in front of the model were analyzed; three of these were along the centerline and the fourth was along the 135° azimuth. Approximately twice as many BVI impulses were recorded at 25° below the rotor plane as at 13° below the rotor plane. The higher intensity BVI impulses, with a pressure rise greater than 200 dynes/cm$^2$, clustered more toward the 135° azimuth than toward the centerline azimuth.

NASA Langley Research Center
Hampton, VA 23665-5225
December 9, 1986

## References

1. Martin, R. M.; Elliott, J. W.; and Hoad, D. R.: Comparison of Experimental and Analytical Predictions of Rotor Blade-Vortex Interactions Using Model Scale Acoustic Data. AIAA-84-2269, Oct. 1984.
2. Boxwell, D. A.; and Schmitz, F. H.: Full-Scale Measurements of Blade-Vortex Interaction Noise. *J. American Helicopter Soc.*, vol. 27, no. 4, Oct. 1982, pp. 11–27.
3. Schmitz, F. H.; and Yu, Y. H.: *Helicopter Impulsive Noise: Theoretical and Experimental Status.* NASA TM-84390, USAAVRADCOM-TR-83-A-2, 1983.
4. Hoad, Danny R.; and Connor, David A.: Acoustic Performance Evaluation of an Advanced UH-1 Helicopter Main Rotor System. Preprint 81-58, *Proceedings of the 37th Annual Forum,* American Helicopter Soc., May 1981.
5. Hoad, Danny R.; Elliott, Joe W.; and Orie, Nettie M.: *Rotor Performance Characteristics From an Aeroacoustic Helicopter Wind-Tunnel Test Program.* NASA TM-87661, AVSCOM TM 86-B-1, 1986.
6. Martin, R. M.; and Connor, Andrew B.: *Wind-Tunnel Acoustic Results of Two Rotor Models With Several Tip Designs.* NASA TM-87698, 1986.
7. Gessow, Alfred; and Myers, Garry C., Jr.: *Aerodynamics of the Helicopter.* Macmillian Co., c.1952. (Republished 1967 by Frederick Ungar Publ. Co.)
8. Heyson, Harry H.: *Use of Superposition in Digital Computers To Obtain Wind-Tunnel Interference Factors for Arbitrary Configurations, With Particular Reference to V/STOL Models.* NASA TR R-302, 1969.
9. Connor, Andrew B.; and O'Bryan, Thomas C.: *A Brief Evaluation of Helicopter Wake as a Potential Operational Hazard to Aircraft.* NASA TN D-1227, 1962.

Table I. Details of Model Rotors

| | |
|---|---|
| Hub type | Fully articulated |
| Number of blades | Four |
| Airfoil section | See figure 2(a) |
| Hinge offset, cm (in.) | 7.6 (3.0) |
| Root cutout, cm (in.): | |
| High-twist rotor | 18.6 (7.3) |
| Low-twist rotor | 25.9 (10.2) |
| Pitch-flap coupling angle, deg | -2 |
| Twist | See figure 2(b) |
| Radius, cm (in.): | |
| High-twist rotor | 142.8 (56.2) |
| Low-twist rotor | 142.3 (56.0) |
| Chord, cm (in.): | |
| High-twist rotor | 9.1 (3.6) |
| Low-twist rotor | 7.9 (3.1) |

Table II. Sample Data of BVI Impulses Generated by Low-Twist Blade Rotor

[Data are from 50- and 60-knot cases]

| $V$, knots | $T$, lb | $\alpha_{TPP}$, deg | Microphone | BVI, dynes/cm$^2$ | Time of occurrence, fraction of rotation |
|---|---|---|---|---|---|
| 50.01 | 483.52 | 8.22 | 5 | 165.1 | 0.292 to 0.302 |
| 50.01 | 483.52 | 8.22 | 12 | 127.9 | .479 to .486 |
| 50.24 | 494.64 | 7.75 | 3 | 394.5 | .098 to .108 |
| 50.24 | 494.64 | 7.75 | 4 | 231.4 | .208 to .218 |
| 50.24 | 494.64 | 7.75 | 5 | 275.9 | .254 to .260 |
| 50.24 | 494.64 | 7.75 | 12 | 254.9 | .380 to .388 |
| 50.40 | 492.39 | 9.54 | 3 | 215.2 | .150 to .158 |
| 50.40 | 492.39 | 9.54 | 5 | 182.3 | .002 to .009 |
| 50.35 | 498.05 | 3.63 | 3 | 252.5 | .682 to .688 |
| 50.35 | 498.05 | 3.63 | 4 | 169.5 | .784 to .791 |
| 50.35 | 498.05 | 3.63 | 5 | 215.7 | .799 to .807 |
| 50.64 | 496.13 | 7.72 | 3 | 226.9 | .686 to .689 |
| 50.64 | 496.13 | 7.72 | 5 | 187.6 | .800 to .808 |
| 50.32 | 499.48 | 9.77 | 12 | 126.8 | .697 to .705 |
| 50.32 | 499.48 | 9.77 | 3 | 290.1 | .197 to .203 |
| 60.24 | 479.42 | 8.02 | 3 | 210.2 | .322 to .330 |
| 60.24 | 479.42 | 8.02 | 12 | 191.3 | .096 to .102 |
| 60.15 | 489.16 | 9.91 | 5 | 133.7 | .244 to .251 |
| 60.15 | 489.16 | 9.91 | 12 | 275.2 | .129 to .138 |
| 60.64 | 496.12 | 5.88 | 12 | 132.8 | .099 to .104 |
| 60.65 | 490.93 | 9.67 | 3 | 311.6 | .099 to .106 |
| 60.65 | 490.93 | 9.67 | 4 | 245.1 | .238 to .248 |
| 60.65 | 490.93 | 9.67 | 5 | 195.3 | .025 to .032 |
| 60.65 | 490.93 | 9.67 | 12 | 148.2 | .143 to .146 |
| 60.43 | 494.86 | 9.83 | 12 | 148.3 | .158 to .159 |

Table III. Statistics of BVI Occurrences by Rotor Type and Microphone Position

(a) Low-twist-rotor BVI impulse occurrences

| Microphone | $\theta$, deg | Occurrences at acoustic pressure of— | | |
|---|---|---|---|---|
| | | <200 dynes/cm$^2$ | >200 dynes/cm$^2$ | Total |
| 3 | 44 | 11 | 12 | 23 |
| 4 | 13 | 6 | 6 | 12 |
| 5 | 23 | 10 | 13 | 23 |
| 12 | 25 | 19 | 10 | 29 |
| Sum . . . . . | | 46 | 41 | 87 |

(b) High-twist-rotor BVI impulse occurrences

| Microphone | $\theta$, deg | Occurrences at acoustic pressure of— | | |
|---|---|---|---|---|
| | | <200 dynes/cm$^2$ | >200 dynes/cm$^2$ | Total |
| 3 | 44 | 7 | 4 | 11 |
| 4 | 13 | 5 | 3 | 8 |
| 5 | 23 | 5 | 10 | 15 |
| 12 | 23 | 8 | 7 | 15 |
| Sum . . . . . | | 25 | 24 | 49 |

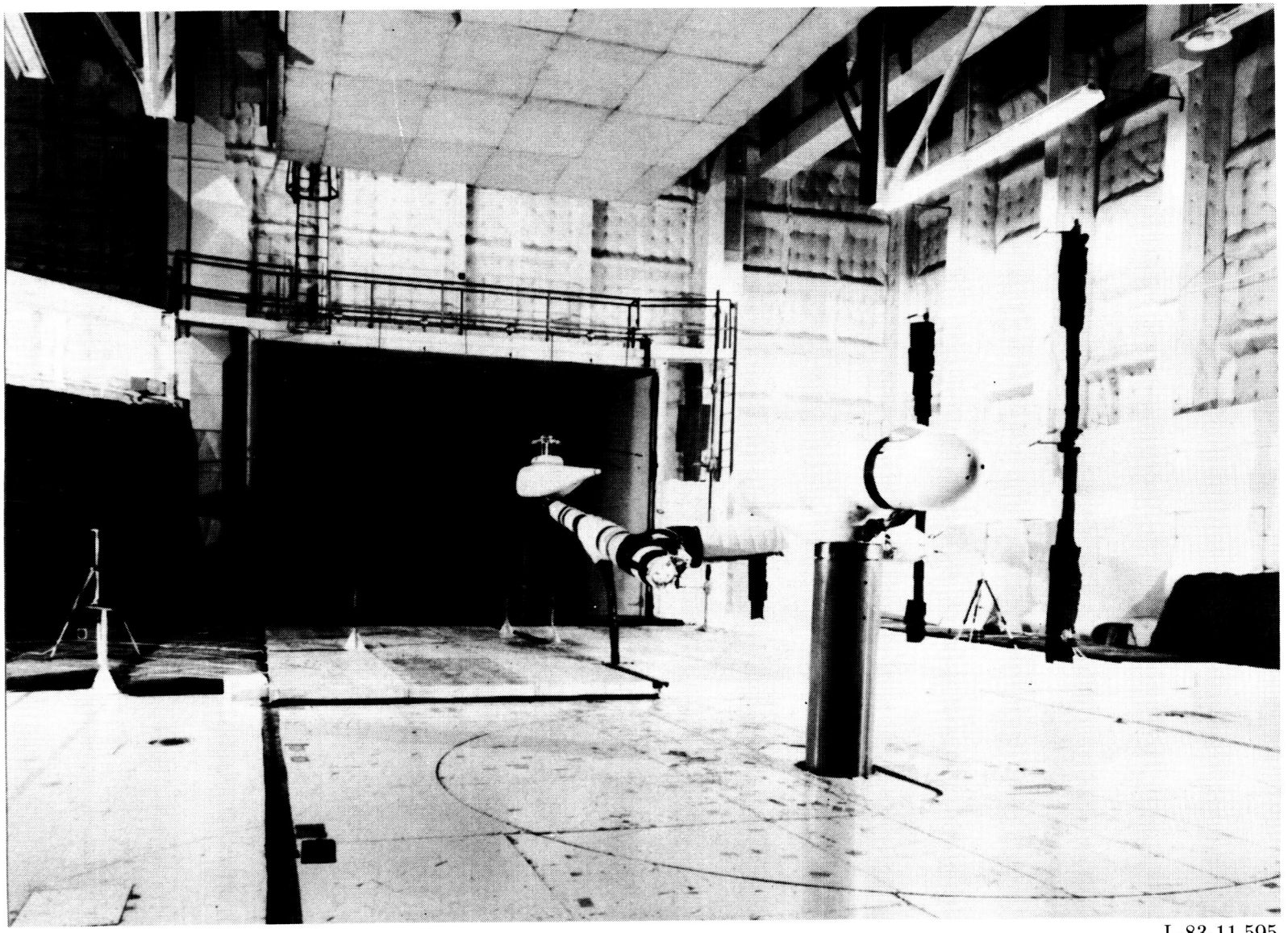

L-83-11,595

(a) View looking upstream.

Figure 1. Photographs of main rotor model and test rig sting mounted in the Langley 4- by 7-Meter Tunnel.

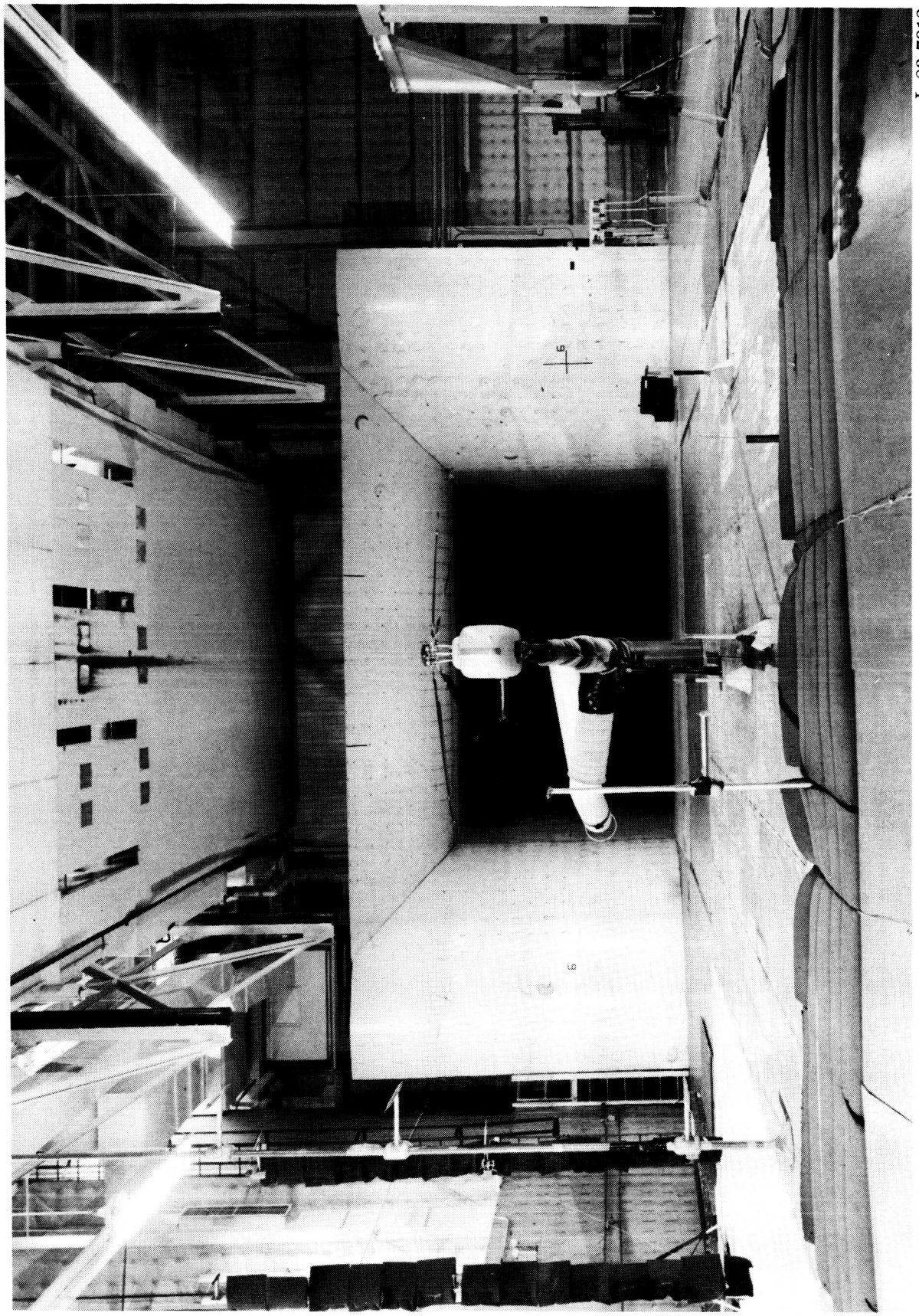

L-83-7012

(b) View looking downstream.

Figure 1. Concluded.

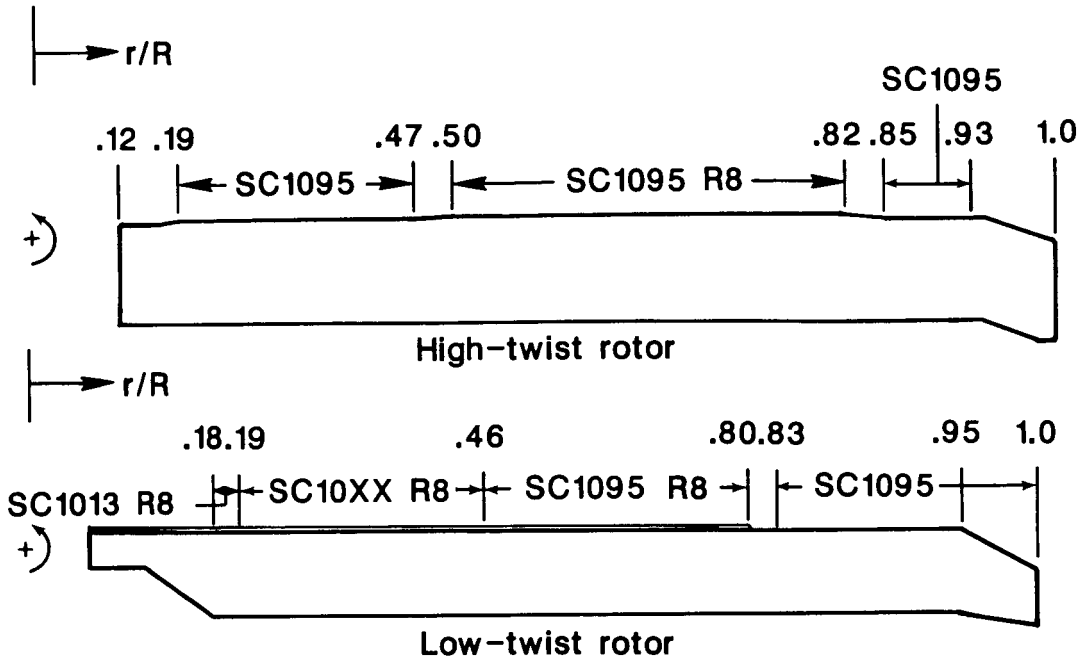


(a) Rotor blade planform.

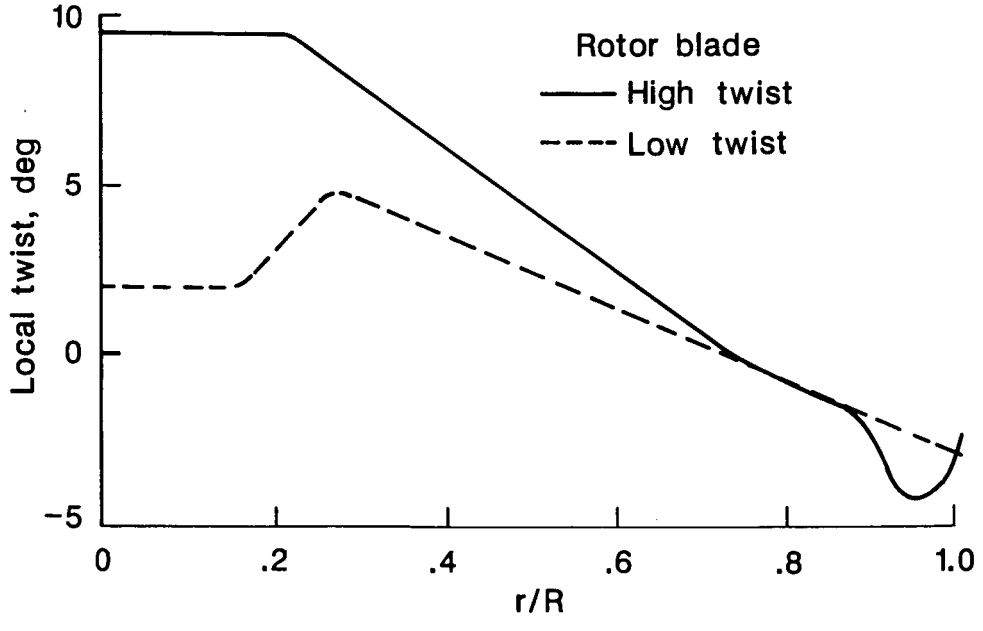


(b) Rotor blade twist distribution.

Figure 2. General description of two rotor models showing blade planform, airfoil section, and twist distribution.

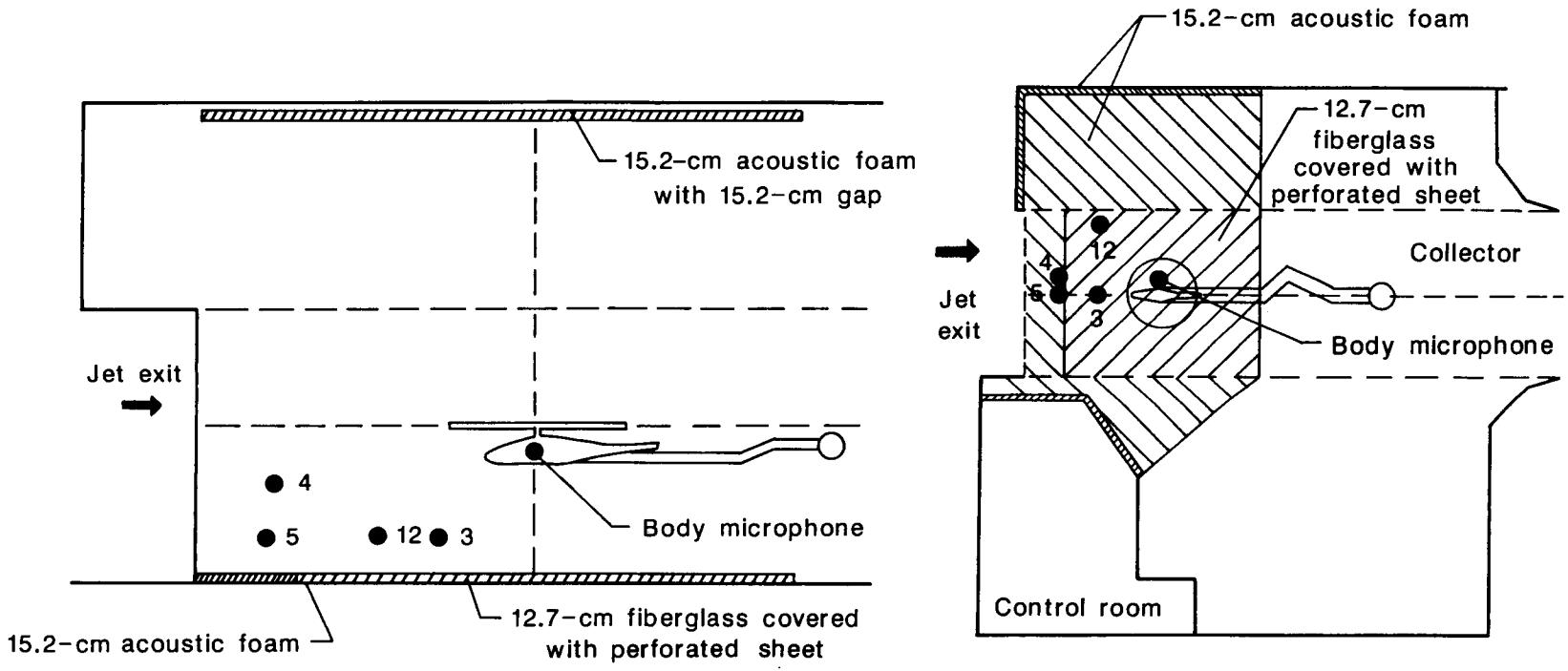


(a) Elevation.

(b) Planview.

Figure 3. Sketch showing microphone positions in relation to rotor model.

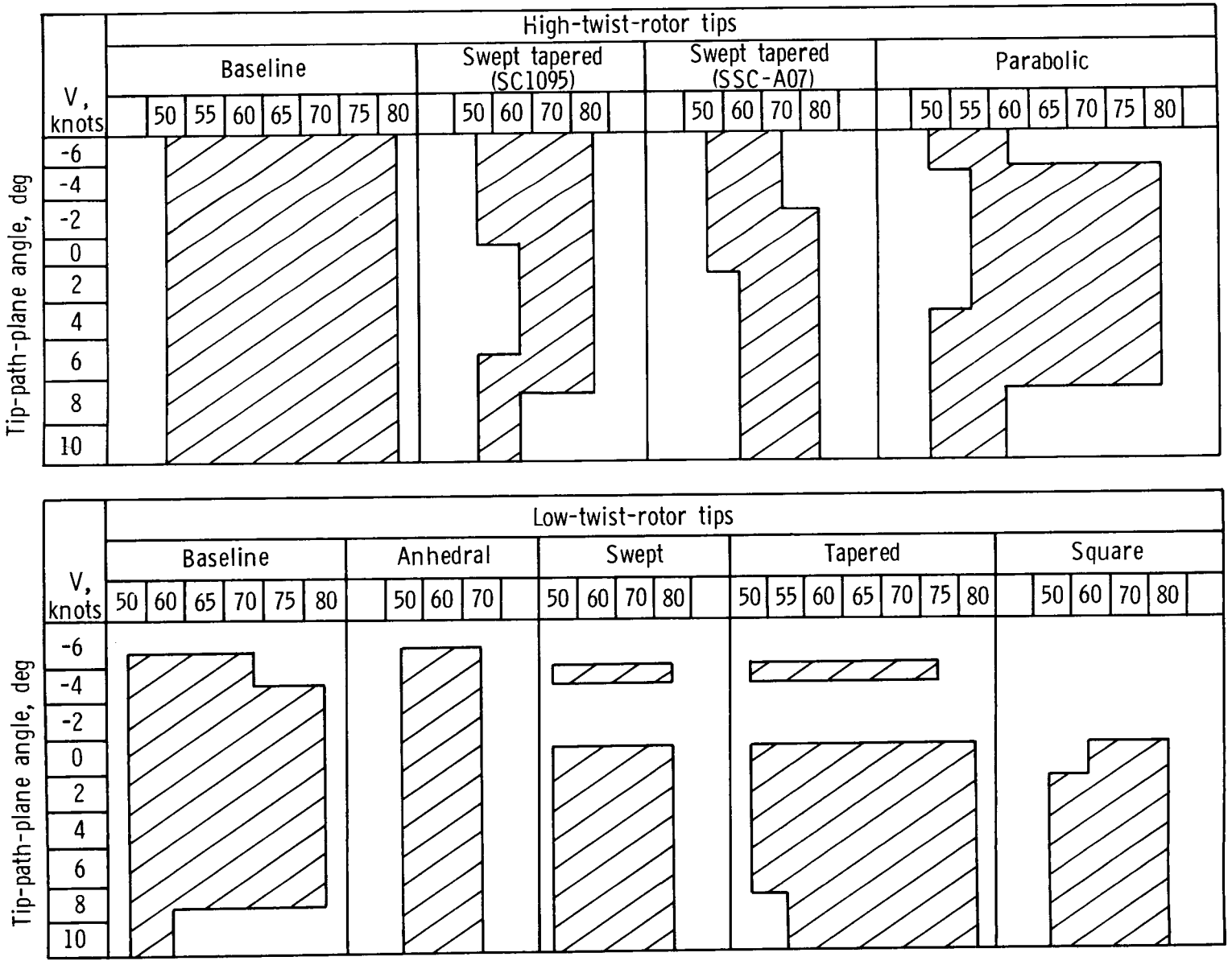


Figure 4. Matrix diagram of test conditions for each rotor.

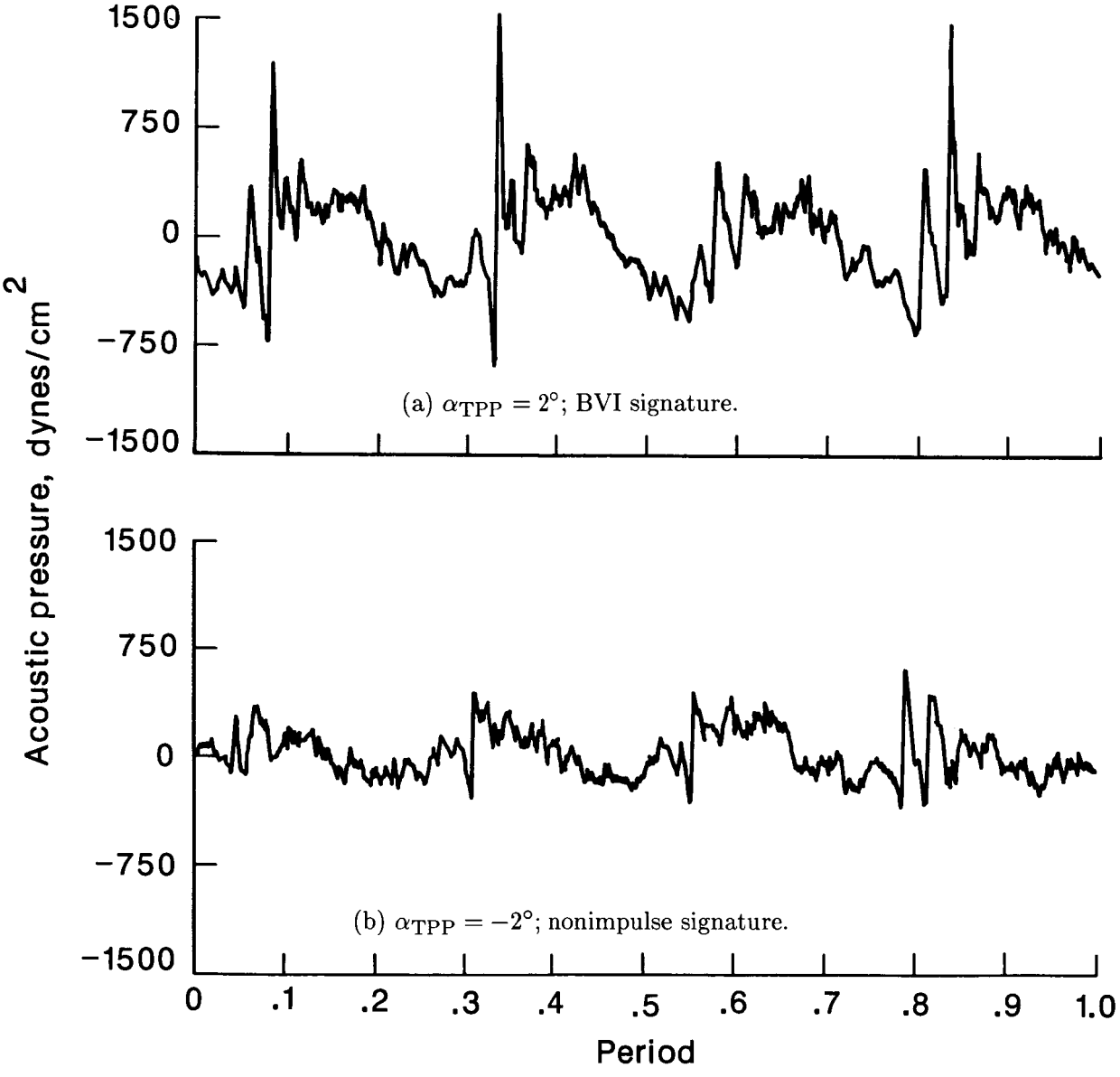


Figure 5. Typical acoustic pressure time histories for one rotor rotation at $V = 70$ knots.

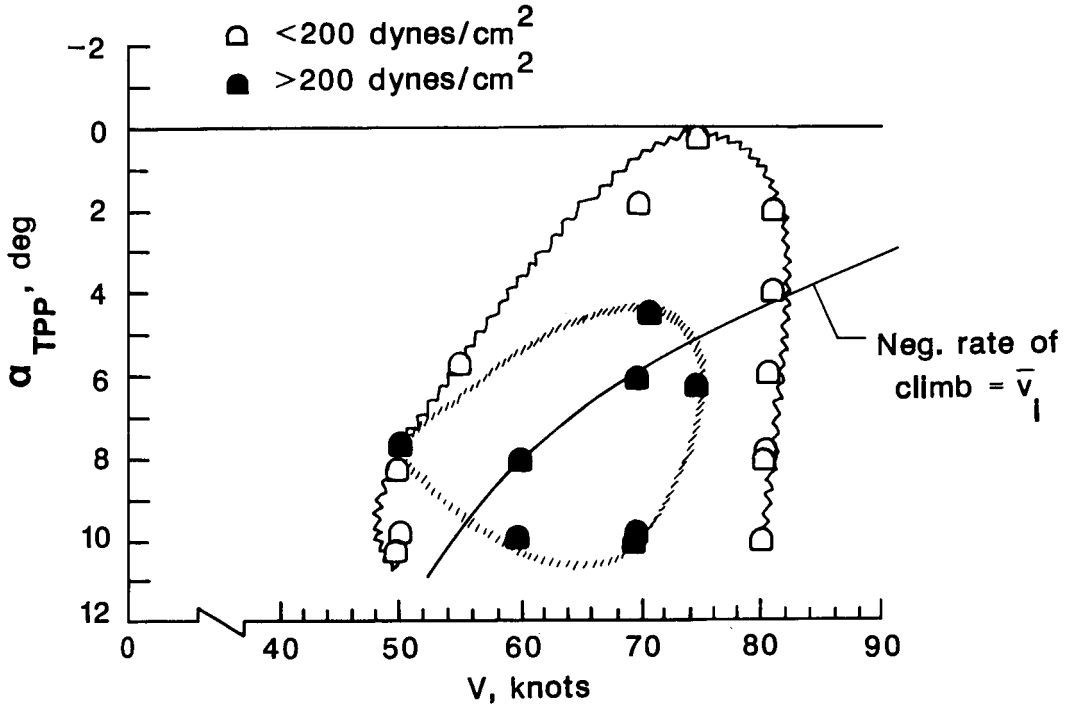


(a) Microphone 12. $r = 12.98$ ft; $\theta = 25°$; $\psi = 133°$.

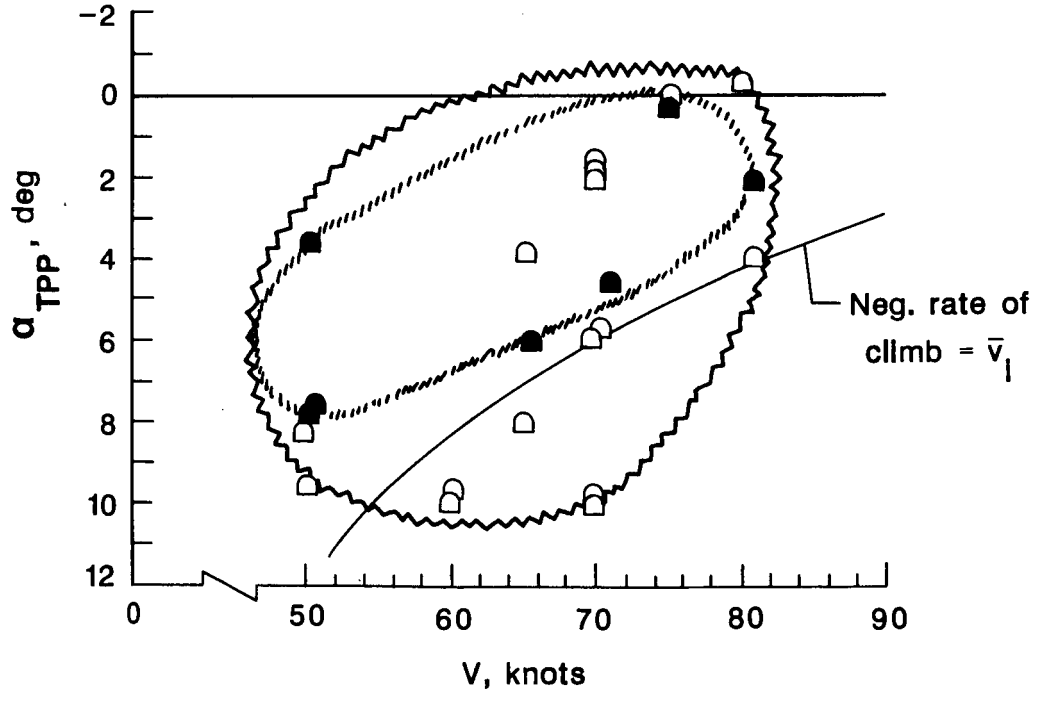


(b) Microphone 5. $r = 14.52$ ft; $\theta = 23°$; $\psi = 177°$.

Figure 6. Plot of BVI impulse occurrences from low-twist rotor as function of $V$ versus $\alpha_{TPP}$.

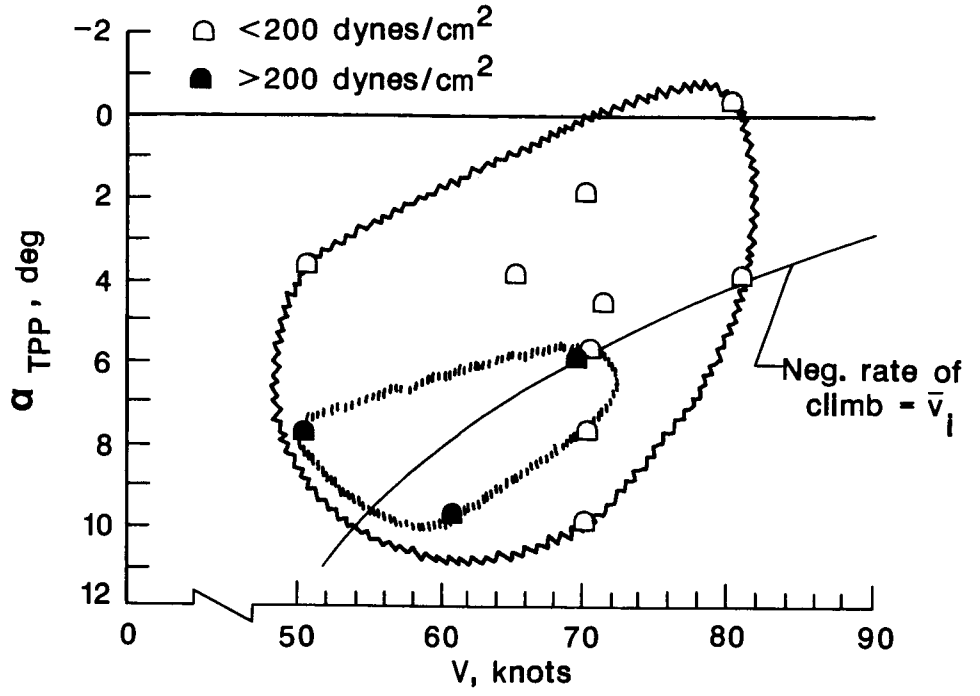


(c) Microphone 4. $r = 13.99$ ft; $\theta = 13°$; $\psi = 172°$.

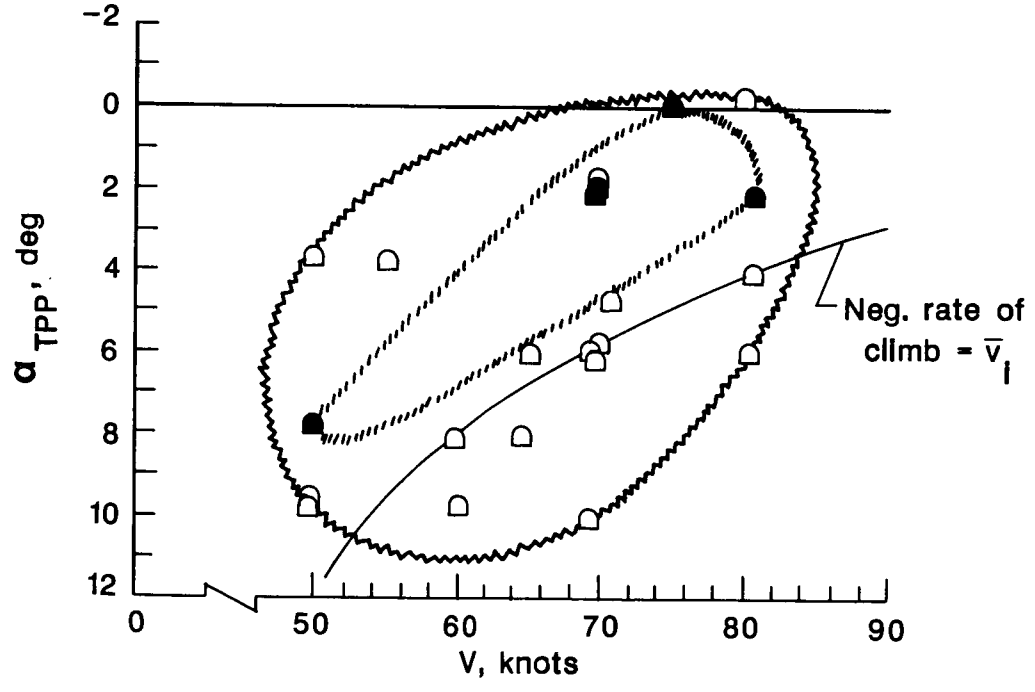


(d) Microphone 3. $r = 8.28$ ft; $\theta = 44°$; $\psi = 176°$.

Figure 6. Concluded.

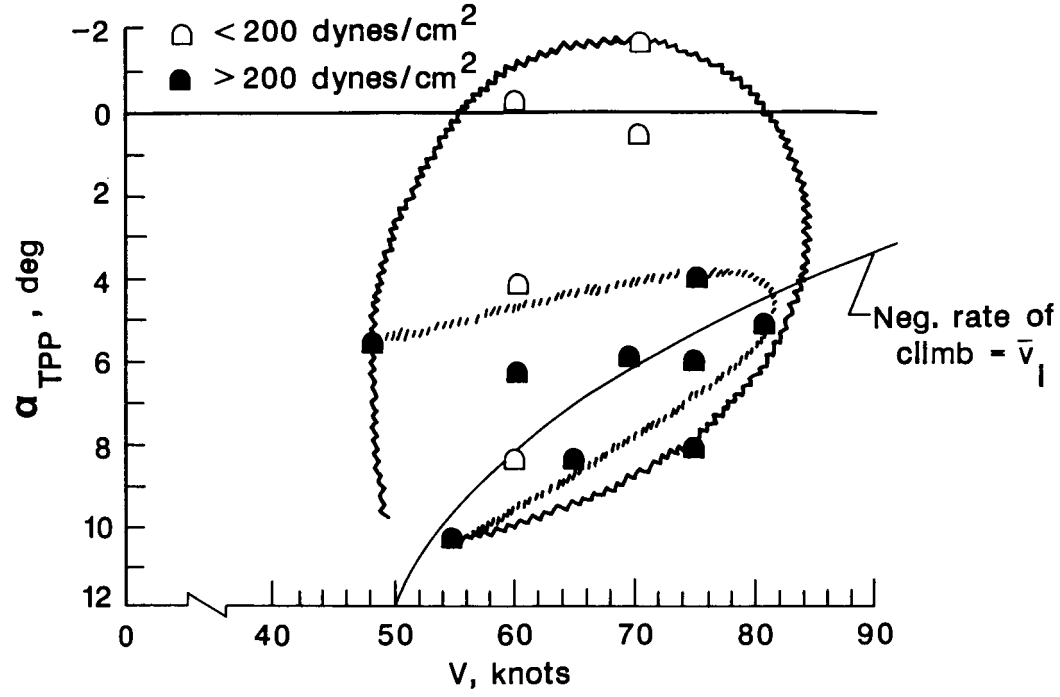


(a) Microphone 12. $r = 12.98$ ft; $\theta = 25°$; $\psi = 133°$.

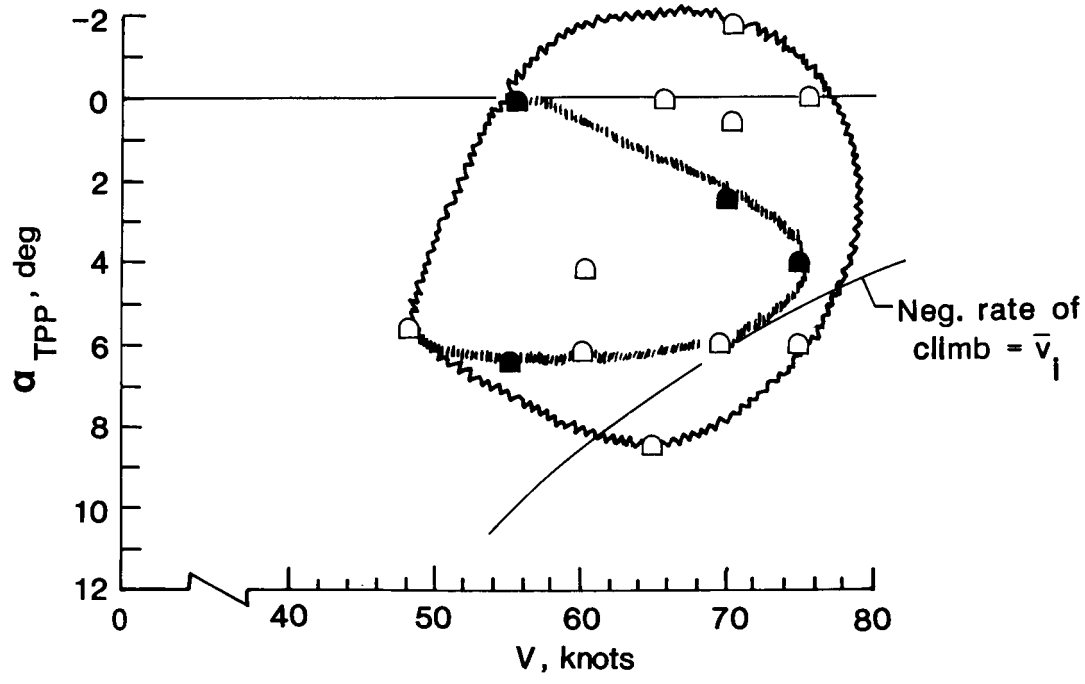


(b) Microphone 5. $r = 14.52$ ft; $\theta = 23°$; $\psi = 177°$.

Figure 7. Plot of BVI impulse occurrences from high-twist rotor as function of $V$ versus $\alpha_{\mathrm{TPP}}$.

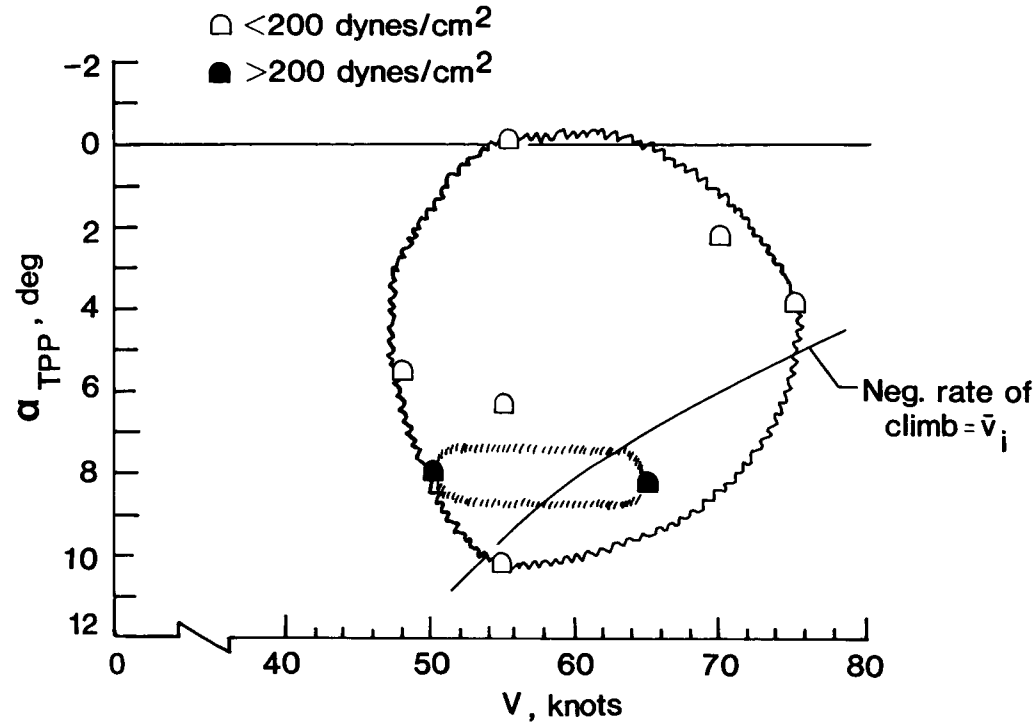


(c) Microphone 4. $r = 13.99$ ft; $\theta = 13°$; $\psi = 172°$.

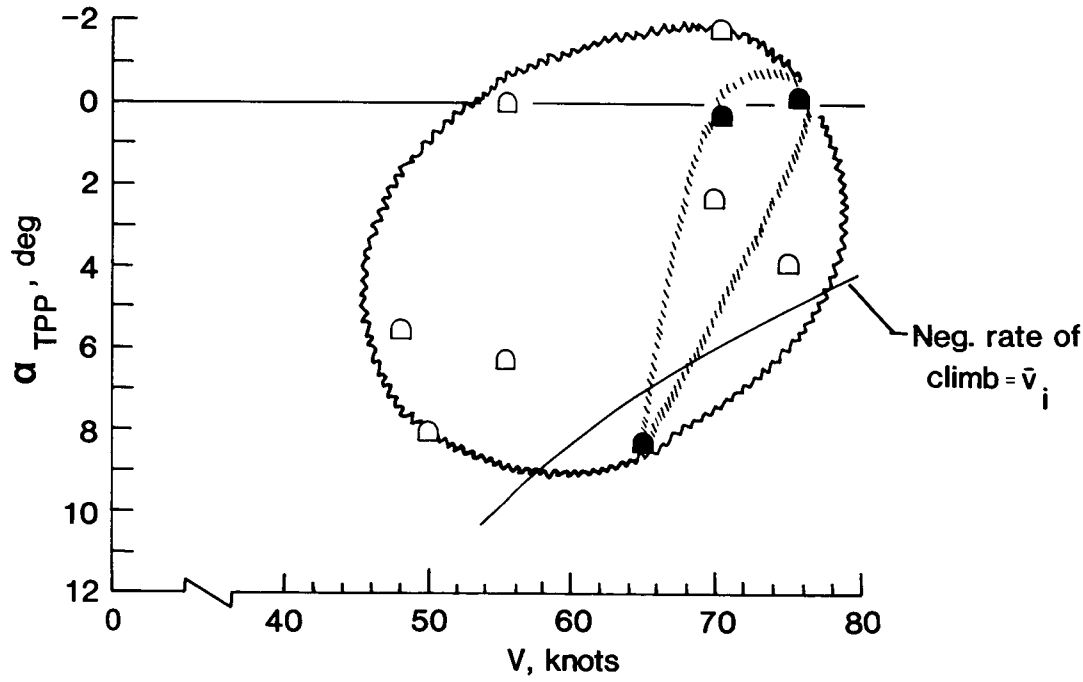


(d) Microphone 3. $r = 8.28$ ft; $\theta = 44°$; $\psi = 176°$.

Figure 7. Concluded.

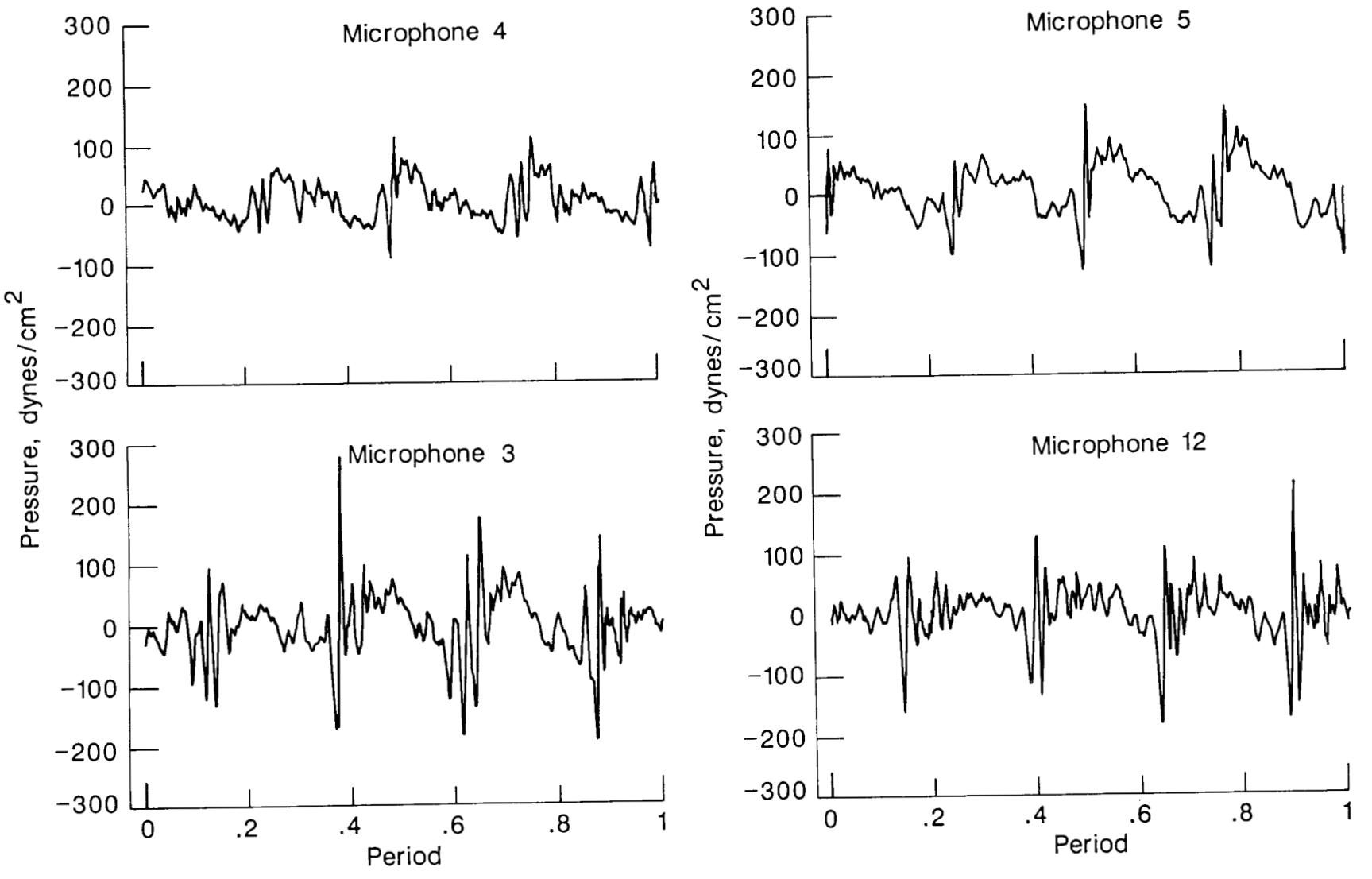


Figure 8. Instantaneous pressure time histories from one test condition showing difference in signature at each of four forward-position microphones analyzed.

Standard Bibliographic Page

| 1. Report No. | 2. Government Accession No. | 3. Recipient's Catalog No. |
|---|---|---|
| NASA TP-2650 | | |

| 4. Title and Subtitle | 5. Report Date |
|---|---|
| Correlation of Helicopter Impulsive Noise From Blade-Vortex Interaction With Rotor Mean Inflow | March 1987 |
| | 6. Performing Organization Code: 505-61-51 |
| 7. Author(s): Andrew B. Connor and R. M. Martin | 8. Performing Organization Report No.: L-16145 |
| 9. Performing Organization Name and Address: NASA Langley Research Center, Hampton, VA 23665-5225 | 10. Work Unit No. |
| | 11. Contract or Grant No. |
| 12. Sponsoring Agency Name and Address: National Aeronautics and Space Administration, Washington, DC 20546-0001 | 13. Type of Report and Period Covered: Technical Paper |
| | 14. Sponsoring Agency Code |

15. Supplementary Notes

16. Abstract

Data from a test made in the Langley 4- by 7-Meter Tunnel were parametrically studied with respect to the occurrence of blade-vortex interaction (BVI) as a function of tunnel speed and rotor angle of attack. Three microphones on the tunnel centerline forward of the model and one microphone forward and 45° to the right provided the data for this study. The rotor model was tested with a set of high-twist blades (−10°) and a set of low-twist blades (−5°) over the midspeed range (50 to 80 knots) at angles of attack ranging from −6° (shallow climb) to 10° (steep descent). The data from all four microphones indicated that the most probable time of occurrence of BVI is when the rotor descent is approximately equal to the rotor mean inflow velocity. However, some of the data showed no conclusive relationship to the mean inflow velocity.

| 17. Key Words (Suggested by Authors(s)) | 18. Distribution Statement |
|---|---|
| Helicopter<br>Wind-tunnel test<br>Blade-vortex-interaction noise | Unclassified—Unlimited<br><br>Subject Category 71 |

| 19. Security Classif.(of this report) | 20. Security Classif.(of this page) | 21. No. of Pages | 22. Price |
|---|---|---|---|
| Unclassified | Unclassified | 21 | A02 |

For sale by the National Technical Information Service, Springfield, Virginia 22161

NASA-Langley, 1987